Development of brain PET using GAPD arrays

Jin Ho Jung, Yong Choi,[a] Key Jo Hong, Jihoon Kang, Wei Hu, Hyun Keong Lim, Yoonsuk Huh, Sangsu Kim, Jiwoong Jung, and Kyu Bom Kim
Department of Electronic Engineering, Sogang University, 1 Shinsu-Dong, Mapo-Gu, Seoul 121-742, Korea and Department of Nuclear Medicine, Samsung Medical Center, Sungkyunkwan University School of Medicine, 50 Ilwon-Dong, Gangnam-Gu, Seoul 135-710, Republic of Korea

(Received 21 July 2011; revised 17 November 2011; accepted for publication 11 January 2012; published 15 February 2012)

Purpose: In recent times, there has been great interest in the use of Geiger-mode avalanche photodiodes (GAPDs) as scintillator readout in positron emission tomography (PET) detectors because of their advantages, such as high gain, compact size, low power consumption, and magnetic field insensitivity. The purpose of this study was to develop a novel PET system based on GAPD arrays for brain imaging.
Methods: The PET consisted of 72 detector modules arranged in a ring of 330 mm diameter. Each PET module was composed of a 4×4 matrix of $3 \times 3 \times 20$ mm^3 cerium-doped lutetium yttrium orthosilicate (LYSO) crystals coupled with a 4×4 array three-side tileable GAPD. The signals from each PET module were fed into preamplifiers using a 3 m long flat cable and then sent to a position decoder circuit (PDC), which output a digital address and an analog pulse of the interacted channel among 64 preamplifier signals tranmitted from four PET detector modules. The PDC outputs were fed into field programmable gate array (FPGA)-embedded data acquisition (DAQ) boards. The analog signal was then digitized, and arrival time and energy of the signal were calculated and stored.
Results: The energy and coincidence timing resolutions measured for 511 keV gamma rays were $18.4 \pm 3.1\%$ and 2.6 ns, respectively. The transaxial spatial resolution and sensitivity in the center of field of view (FOV) were 3.1 mm and 0.32% cps/Bq, respectively. The rods down to a diameter of 2.5 mm were resolved in a hot-rod phantom image, and activity distribution patterns between the white and gray matters in the Hoffman brain phantom were well imaged.
Conclusions: Experimental results indicate that a PET system can be developed using GAPD arrays and the GAPD-based PET system can provide high-quality PET imaging. © *2012 American Association of Physicists in Medicine*. [DOI: 10.1118/1.3681012]

Key words: GAPD arrays, LYSO, position decoder circuit, PET, brain imaging

I. INTRODUCTION

The Geiger-mode avalanche photodiodes (GAPDs) are solid-state photosensors consisting of an array of microavalanche photodiodes (APDs) that operate in limited Geiger mode. Each micro-APD, referred to as a "microcell," produces a pulse signal when it detects one photon. The final output of the GAPD is the sum of the outputs from each microcell.[1,2] The GAPDs have various advantages over other conventional photosensors such as APDs or photomultiplier tubes (PMTs). In comparison to the APDs, the GAPDs produce a high gain ($\sim 10^6$) signal with high signal-to-noise ratio and also offer a fast response with a rise time of less than l ns. The GAPDs also have advantages over the PMTs because of their compactness, low bias voltage requirement, and insensitivity to magnetic fields. In addition, the GAPDs have the potential to become less expensive compared with the APDs and PMTs because they can be fabricated using a standard complementary metal–oxide–semiconductor (CMOS) process.[3–6]

In the last few years, various single-channel GAPDs with different active areas or numbers of microcells have been developed, and feasibility tests of the GAPDs as a photosensor for PET applications have been carried out.[7–12] Several groups have demonstrated the usefulness of GAPDs in PET applications. However, the early GAPDs had several limiting features such as low fill-factor, small active area, low photon detection efficiency, and high dark count rate. Recently, 2D arrays of single-channel GAPDs in a common substrate have been fabricated by a few research groups and manufacturers.[13–16] This has improved fill-factor, photon detection efficiency in the blue wavelength region, and optical cross-talk. These GAPD arrays allow construction of a PET scanner having a meaningful field of view (FOV), assuring acceptable detection efficiency for gamma rays.[17,18]

The purpose of this study was to develop a novel PET system based on GAPD arrays for human brain imaging. In addition, as the development of a PET-MRI hybrid imaging instrumentation is also under investigation by our group, the PET in this work is designed such that it is capable of operating inside and outside MRI. The PET detector modules consisting of cerium-doped lutetium yttrium orthosilicate (LYSO) and GAPD arrays were fabricated to demonstrate that the GAPD arrays could be used in human PET system development. Analog and digital electronic circuits

dedicated to GAPD-based PET detectors were designed and constructed. Energy, time and spatial resolutions, and sensitivity were measured to evaluate the performance of the proposed PET system. Hot-rod and Hoffman-brain phantom images were also acquired to demonstrate the imaging performance of the prototype PET based on GAPD arrays.

II. MATERIALS AND METHODS

II.A. Brain PET design and fabrication

II.A.1. PET detector module

The PET detector module designed in this study consisted of a LYSO (Sinoceramics, Shanghai, China) scintillator block coupled to a 4×4 array GAPD (SensL, Cork, Ireland), as shown in Fig. 1(a). The scintillator block was composed of a 4×4 matrix of $3 \times 3 \times 20$ mm^3 crystals. The individual crystal elements were mechanically polished on all sides and optically isolated with a 0.3 mm white epoxy resin. Each pixel of the GAPD array had a 2.85×2.85 mm^2 sensitive area; 3640 micropixels; and 3.3 mm pitch. The GAPD was operated at a bias voltage of 32.5 V to achieve a gain of about 3.5×10^6. The scintillator was directly coupled to the GAPD without optical-coupling material. Each PET detector module was encapsulated from light.

II.A.2. Analog signal processing

The signals from each PET detector module were fed into 16-channel preamplifiers using a 3 m long flexible flat cable (FFC), as shown in Fig. 1(b), and amplified up to 1000 times. The amplitude, rise time, and fall time of the amplified signal generated by a 511 keV gamma ray were about 250 mV, 30 ns, and 170 ns, respectively.

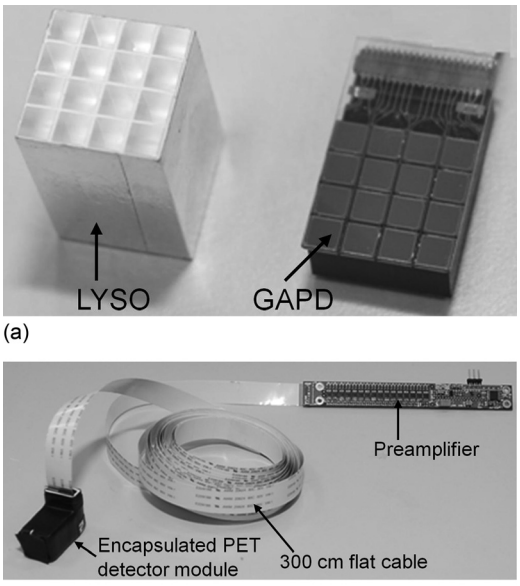

FIG. 1. (a) A 4×4 matrix of $3 \times 3 \times 20$ mm^3 LYSO crystals and a 4×4 array GAPD used to construct PET detector module and (b) the PET detector module and preamplifier connected using a 300 cm long flexible flat cable.

The amplified signals were sent to a position decoder circuit (PDC), which output the channel address and the analog pulse of the interacted channel with a coincidence event among 64 amplified signals transmitted from four detector modules. Previously, 32:1 PDC dedicated to PET application had been successfully developed and evaluated.[19] The 64:1 PDC used in this study was fabricated by connecting two modified 32:1 PDCs. The primary functions such as input offset voltage level control, gain adjustment, signal delay, energy discrimination, signal switching, and digital signal processing were implemented in the modified PDC. Moreover, an additional function, which held the PDC outputs by an external trigger, was implemented. The interacted channel among 32 outputs from 2 detector modules was independently identified using each 32:1 PDC, and then the trigger signal from each PDC was generated. In the previous study, we demonstrated that the fastest signal had a high probability of being a valid signal generated from the interacted channel. Thus, a faster trigger signal would be generated by one of the two 32:1 PDCs and transferred to the other PDC. As a result, the other PDC outputs would be held, as illustrated in Fig. 2(a). The analog pulse, 5-bit channel address, and 1-bit PDC board ID corresponding to the interacted channel were transferred from the valid PDC to the data acquisition (DAQ) module. These output signals were delayed about 50 ns compared with the input signal. No meaningful distortion of the analog output signal was observed. The PDC was reset using the trigger signal transmitted from the DAQ module.

II.A.3. Digital signal processing

The DAQ module (VHS-ADC Virtex-4, Lyrtech, Inc., Quebec, Canada) shown in Fig. 2(c), which had 8-channel ADCs with a maximum sampling rate of 105 MHz, a field programmable gate array (FPGA) with 104 MHz on-board clock, 64-bit digital I/O, and a 128 MB SDRAM, was used to process output signals from the PDC. Further, 2GB SDRAM was added to the module for recording large amounts of data. The analog output signal of the PDC was digitized by 100 MHz free-running ADC. The energy of the detected gamma ray was calculated by integrating the digitized pulse, and the arrival time was determined from the rising time of the digital signal.[20] Data were stored in list mode format (LMF) on the host computer for coincidence sorting and image reconstruction. In addition, a trigger signal was generated to reset the PDC after 320 ns for digitization of the analog signal.

II.A.4. Brain PET using GAPD arrays

In this study, a prototype PET system dedicated to human brain imaging, as shown in Fig. 3(a), was designed and constructed. The brain PET consisted of 72 detector modules arranged in a ring of 330 mm diameter. In all, 1152 channel outputs from 72 detector modules were sent to seventy-two 16-channel preamplifier circuits, and then preamplified signals were transmitted to 18 PDCs. Eighteen analog signals (18 PDCs $\times$ 1 signal/PDC) and eighteen 6-bit digital signals from the 18 PDCs were sent to three DAQ modules. External

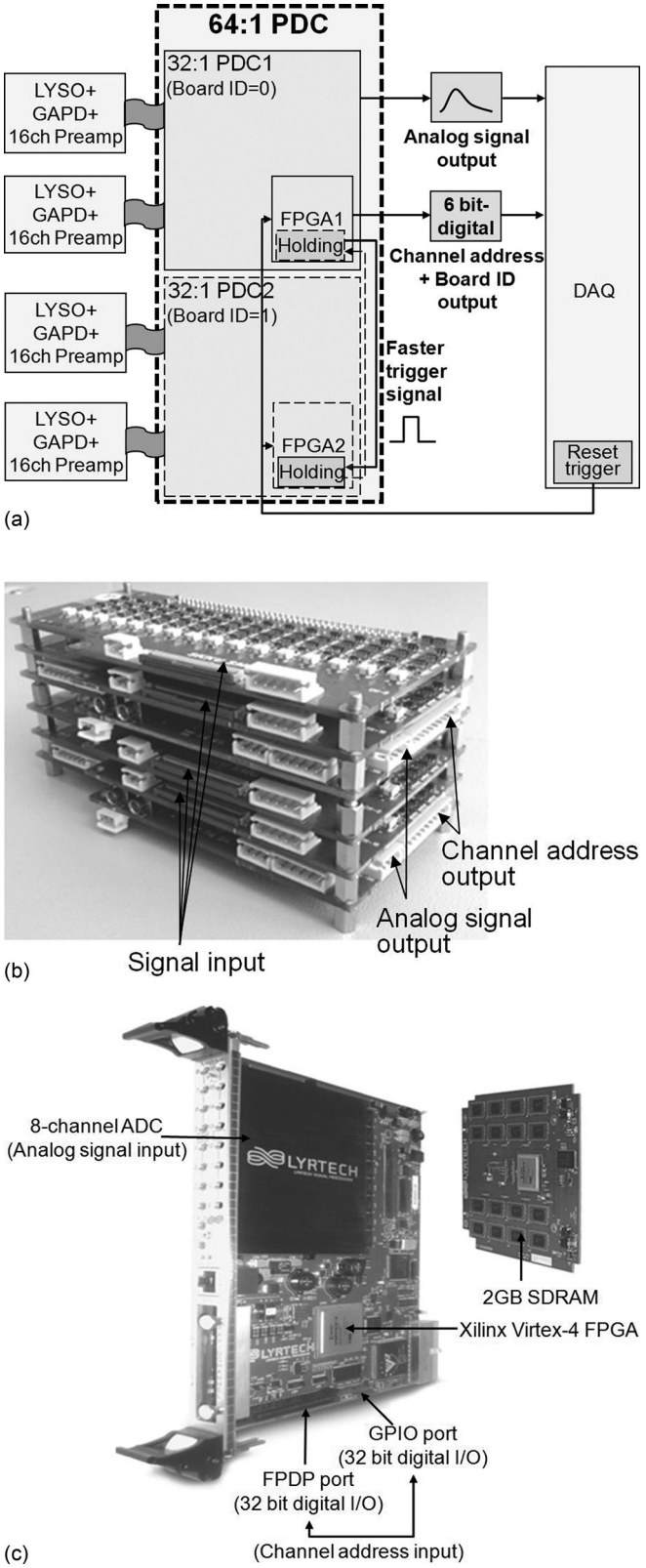

FIG. 2. (a) Signal processing scheme and (b) photograph of the fabricated 64:1 position decoder circuit (PDC) and (c) the data acquisition (DAQ) module used for digital signal processing. The outputs of the 32:1 PDC with a slower trigger signal was held by a trigger signal transmitted from the other 32:1 PDC with a faster trigger signal, and then an analog pulse, channel address, and PDC board ID of the interacted (faster trigger signal) channel were transferred from the PDC to the DAQ module. The DAQ module consisted of 8-channel free-running ADC, digital I/O port, FPGA, and 2GB SDRAM.

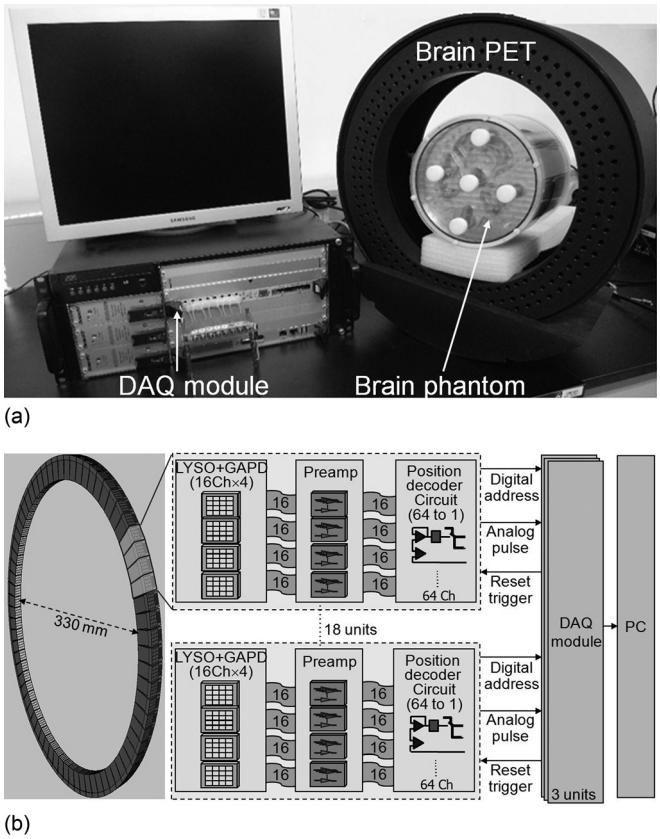

FIG. 3. (a) The prototype brain PET consisting of 72 detector modules arranged in a ring 330 mm in diameter and (b) signal processing architecture of the brain PET system consisting of PET detector modules, analog and digital electronics, and a host PC.

clock signals of 100 MHz were transferred to each DAQ to synchronize the clocks of multiple DAQs. In addition, trigger signals were sent to each DAQ to initialize and to synchronize a counter that works as a timer.

The LMF data acquired by the DAQ modules were transferred to a host computer and then sorted into coincidence data. The two procedures were performed to determine whether the two singles are a coincidence event or not. The first one finds a pair of single events that occur within the time window of 10 ns and within the energy window of 350–650 keV, whereas the other excludes lines of responses (LORs) lying outside the 250-cm transaxial FOV in the PET. The PET sinogram data were acquired using the LORs corresponding to a span of three and were combined into a single sinogram to increase the axial sensitivity. Image reconstruction was performed using 2D filtered backprojection (FBP) applying a Hann filter with a cutoff at 0.5 of the Nyquist frequency. The matrix and pixel sizes of the reconstructed image were 300×300 and 1.16 mm, respectively. The aforementioned reconstruction parameters were used to analyze all experimental data.

Figure 3(b) illustrates the signal processing architecture of the brain PET consisting of PET detector modules, analog and digital electronics, and a host PC. The temperature of the PET detector modules was stabilized to room temperature (24 °C) by an air-circulating fan and was monitored

throughout the measurements by a microprocessor-based digital thermometer.

II.B. Performance measurement of the prototype PET

II.B.1. Energy and timing resolutions

A ^{22}Na point source with an activity of 810 kBq placed at the center of the FOV of the prototype PET was used to measure the energy and timing spectra. The LMF data for single events were acquired for 10 min.

Individual energy spectra for 1152 output channels of the 72 PET detector modules were acquired, and then energy resolutions of these energy spectra were calculated. The LMF data acquired from whole PET detectors were sorted into coincidence data, and timing spectrum and resolution were measured using these data.

II.B.2. Sensitivity

Sensitivity was measured by moving a ^{22}Na point source with 2 mm increments in the axial direction. The data were acquired for 10 min at each position, and random coincidence data acquired using the delayed window method were subtracted from prompts before the calculation of sensitivity. The sensitivity (S), % cps/Bq, was calculated as follows:[21]

$$S(\%\,\mathrm{cps/Bq}) = \frac{C_p(\mathrm{cps}) - C_r(\mathrm{cps})}{A(Bq) \times F_b} \times 100,$$

where C_p and C_r are prompt and random coincidence count rates, respectively. $A(Bq)$ is the source activity, and F_b is the branching ratio (0.906) of ^{22}Na.

II.B.3. Spatial resolution

A phantom consisting of six capillary tubes (0.6 mm inner diameter, 50 mm length, and 20 mm pitch) was filled with 0.5 MBq ^{18}F and was located at 0, +2, +4, +6, and +8 cm radial offsets from the center of the prototype PET scanner FOV. Phantom data were acquired for 10 min and were then sorted into coincidence data and sinograms. The PET emission sinogram data for six line phantoms were reconstructed, and radial and tangential profiles of the reconstructed image were plotted and fitted with a Gaussian function. The full width at half-maximum (FWHM) of the fitted curve was calculated to evaluate the spatial resolution over the field of view.

II.B.4. Imaging capability

To evaluate the PET imaging capability using the brain PET system based on GAPD arrays, hot-rod and 3D Hoffman brain phantoms were used, and both phantoms were filled with 18.5 MBq ^{18}F. The hot-rod phantom consisted of 40 rods with various diameters of 2.5, 3.5, 4.5, 5.5, and 6.5 mm arranged in five sectors. The hot-rod and brain phantoms data were acquired for 10 and 30 min, respectively.

Before the reconstruction, image corrections were performed to improve the image quality. The direct normalization method, which obtain a correction factor by scanning a uniform source located at the center of the FOV of the scanner and normalizing the number of events in each LOR to an average value for all LORs in the PET scanner, was applied.[22] The normalization data were acquired for 6 h using a cylindrical phantom (215 mm inner diameter and 185 mm length) filled with 18.5 MBq ^{18}F.

The random correction was performed using a delayed window method, which subtract random counts recorded in the delayed coincidence timing window from prompt coincidence counts.[23]

The attenuation correction was achieved by calculating the attenuation length from the shape of the medium assuming that the medium had uniform attenuation coefficient.[24]

The corrected sinograms of the two phantoms were reconstructed using 2D FBP, applying a Hann filter with a cutoff at 0.5 of the Nyquist frequency.

III. RESULTS

III.A. Energy and timing resolutions

Figure 4(a) shows a representative energy spectrum of one detector channel among 1152 energy spectra. The average energy resolution for 511 keV gamma rays was 18.4 ± 3.1% ($n = 1152$).

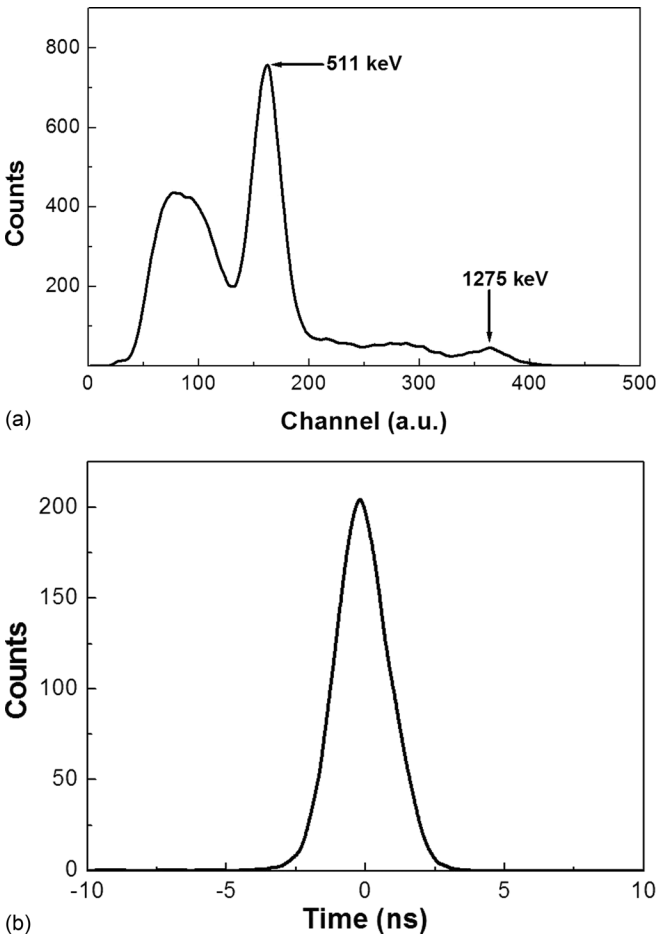

FIG. 4. (a) Energy and (b) timing spectra of one detector channel acquired with a ^{22}Na point source.

The timing spectrum for all coincidence events acquired from 72 PET detector modules is illustrated in Fig. 4(b). The timing resolution of the prototype PET was 2.6 ns.

III.B. Sensitivity

The sensitivity profile as a function of the axial position is shown in Fig. 5(a). The sensitivity was 0.32% at the center of the FOV.

III.C. Spatial resolution

Figure 5(b) shows radial and tangential spatial resolutions of the brain PET as a function of the radial distance from the center of the scanner's FOV. The radial and tangential resolutions of the prototype brain PET varied from 3.1 to 6.4 mm and 3.0 to 3.4 mm when the source was positioned at the center of the FOV and 100 mm off-center, respectively.

III.D. Phantom image

The tomographic images of hot-rod and Hoffman brain phantoms were successfully acquired, as illustrated in Fig. 6.

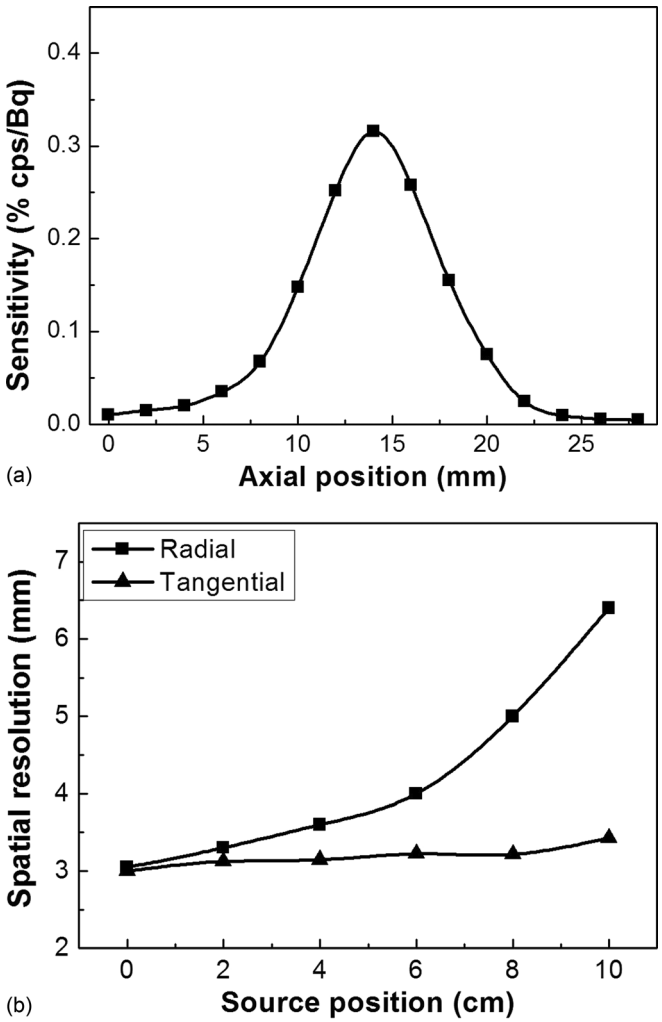

FIG. 5. (a) Sensitivity profile as a function of axial position and (b) radial and tangential spatial resolutions of the brain PET as a function of the radial distance from the center of the scanner FOV.

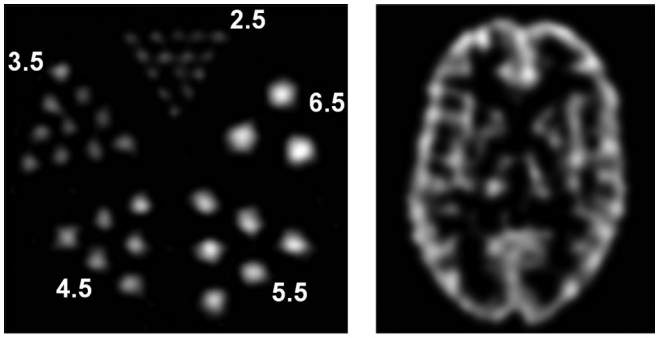

FIG. 6. Tomographic images of (a) hot-rod and (b) 3D Hoffman brain phantoms acquired using the prototype PET.

The rods down to a diameter of 2.5 mm were resolved in a hot-rod phantom image. The activity distribution pattern between white and gray matter in the Hoffman brain phantom was well imaged.

IV. DISCUSSION

In this study, a brain PET system was designed by employing three new design concepts, which used GAPD arrays as a PET photosensor, transmitted the charge signal of the photosensor to the preamplifier through charge transmission cables 3 m in length, and reduced the number of readout channels by a factor of 64 using the PDC.

The GAPD arrays have been proposed as an alternative to a PMT as a photosensor for PET application because of their attractive characteristics, such as high gain, fast response, and low power consumption. The average energy resolution achieved with the GAPD-based PET detector module proposed in this study was 18.4%. This result was slightly worse than those reported by previous studies using PMT or GAPD as a photosensor.[25,26] Energy resolution could be improved by coupling the LYSO to the GAPD with an optical-coupling material.[27,28] However, in this study, optical grease or glue was not applied because it could damage the sensor while modifying the detector configuration, which is likely to be frequently performed during the development of an investigational prototype scanner. The GAPD used in this study permitted a limited extension of $N \times 1$ or $N \times 2$ in the axial direction because it had minimal dead-space on only three sides. The developed prototype PET had a small axial FOV of 1.3 cm, and as a result, the sensitivity was lower than that of the other brain PET with large axial FOV.[29,30] Currently, a PET system that extends the axial FOV using GAPD arrays with minimal dead-space on four sides is under investigation to increase the system sensitivity.

The charge signal transmission method has several advantages when applying it in the magnetic resonance (MR) compatible PET. For example, space constraints caused by physical space limitation of an MR bore could be diminished because only crystal, and GAPD arrays were inserted between radio frequency (RF) and gradient coils, and the subsequent electronics were located outside the MR bore. Generally, PET components inside the MR bore are shielded

using conductive materials in order to prevent the distortions of PET electronic signals caused by the RF signals. On the other hand, eddy currents induced in shielding material lead to a distortion of the MR image. Therefore, the shielding mechanism needs to be carefully designed. Mutual interference between PET and MRI could be minimized by positioning all electronics outside an MR bore because the eddy current will be reduced as a result using less conductive material. The change of energy resolution of the PET detector caused by using the charge transmission method was negligibly small (<3%). Although time information of the PET detector output signal was changed using the charge transmission method, it was not a critical issue in generating a time mark for the coincidence detection in our prototype PET system that employed the DAQ module with a 100 MHz ADC and was previously developed digital timing method.[20,31] The maximum change in the time resolution from 10 to 300 cm was less than 0.3 ns, which was small in the brain PET that did not employ time-of-flight (TOF).

The prototype brain PET consisting of 72 PET detector modules generated 1152 outputs. Because only one coincidence event occurs at a time, most of these outputs contain useless information, such as electrical noise or low-energy scattered events. Therefore, a channel reduction circuit, which outputs analog pulse and digital address of the one interacted channel among 64 outputs of four PET detectors consisting of 4×4 array GAPD, was developed. The circuit led to the construction of a simpler DAQ system, as shown in Fig. 3(b). The DAQ system could be used to a PET with extended axial FOV. The scalability could be achieved by using a PDC with a higher channel reduction ratio and by using additional DAQ modules synchronized with the same clock.

The radial spatial resolution of the developed PET was about twice as degraded at 100 mm off-center of the FOV because of the parallax error caused by the gamma rays obliquely incident to the detector surface at the edge of the FOV. This degradation in the spatial resolution could be improved by using an iterative reconstruction method, with a system matrix that includes a model of the radial blurring present in a PET tomograph[32,33] or by measuring the depth of interaction of the incident gamma rays on the detector surface.[34,35]

Hot-rod and 3D Hoffman brain phantom images were successfully acquired using the developed PET. This result demonstrated that the proposed GAPD-based PET system was able to provide high-quality PET images.

V. CONCLUSIONS

In this study, a PET system composed of a GAPD-based detector module and a dedicated signal processing circuits was designed and fabricated. The experimental results indicated that the PET system could be designed using GAPD arrays, and the developed GAPD-based PET system would be useful for high-quality PET imaging. In addition, PET applied with the charge signal transmission method would allow the design of a compact and lightweight PET insert for hybrid PET-MRI because the PET detector was only composed of LYSO and GAPD arrays without subsequent electronics. Currently, the mechanics and magnetic shielding that are needed to operate the prototype brain PET inside the MR bore are being designed.

ACKNOWLEDGMENTS

This research was supported by the Converging Research Center Program through the Ministry of Education, Science and Technology (Grant No. 2011K000715) and by the Technology Innovation Program funded by the Ministry of Knowledge Economy (Grant No. 10030029), Republic of Korea.

[a]Author to whom correspondence should be addressed. Electronic mail: ychoi.image@gmail.com; also at Department of Electronic Engineering, Sogang University, 1 Sinsu-Dong, Mapo-Gu, Seoul 121-742, Korea. Telephone: 82-2-705-8910; Fax: 82-2-713-2652.

[1]A. N. Otte, J. Barral, B. Dolgoshein, J. Hose, S. Klemin, E. Lorenz, R. Mirzoyan, E. Popova, and M. Teshima, "A test of silicon photomultipliers as readout for PET," Nucl. Instrum. Methods Phys. Res. A **545**, 705–715 (2005).

[2]D. Renker, "Geiger-mode avalanche photodiodes, history, properties and problems," Nucl. Instrum. Methods Phys. Res. A **567**, 48–56 (2006).

[3]P. Buzhana, B. Dolgoshein, E. Garutti, M. Groll, A. Karakash, V. Kaplin, V. Kantserov, F. Kayumov, S. Klyomin, N. Kondratieva, A. Pleshko, E. Popova, and F. Sefkow, "Timing by silicon photomultiplier: A possible application for TOF measurements," Nucl. Instrum. Methods Phys. Res. A **567**, 353–355 (2006).

[4]A. N. Otte, B. Dolgoshein, J. Hose, S. Klemin, E. Lorenz, G. Lutz, R. Mirzoyan, E. Popova, R. H. Richter, L. W. J. Strüder and M. Teshima, "Prospects of using silicon photomultipliers for the astroparticle physics experiments EUSO and MAGIC," IEEE Trans. Nucl. Sci. **53**, 636–640 (2006).

[5]T. K. Lewellen, "Recent developments in PET detector technology," Phys. Med. Biol. **53**, R287–R317 (2008).

[6]R. Lecomte, "Novel detector technology for clinical PET," Eur. J. Nucl. Med. Mol. Imaging **36**, 69–85 (2009).

[7]D. J. Herbert, V. Saveliev, N. Belcari, N. D. Ascenzo, A. Del Guerra, and A. Golovin, "First results of scintillator readout with silicon photomultiplier," IEEE Trans. Nucl. Sci. **53**, 389–394 (2006).

[8]M. McClish, P. Dokhale, J. Christian, C. Stapels, and K. S. Shah, "Characterization and scintillation studies of a solid-state photomultiplier," Nucl. Instrum. Methods Phys. Res. A **572**, 1065–1070 (2007).

[9]V. C. Spanoudaki, A. B. Mann, A. N. Otte, I. Konorov, I. Torres-Espallardo, S. Paul, and S. I. Ziegler, "Use of single photon counting detector arrays in combined PET/MR: Characterization of LYSO-SiPM detector modules and comparison with LSO-APD detector," J. Instrum. **2**, P12002 (2007).

[10]N. Dinu, Z. Amara, C. Bazin, V. Chaumat, C. Cheikali, G. Guilhem, V. Puill, C. Sylvia, and J. F. Vagnucci, "Electro-optical characterization of SiPM: A comparative study," Nucl. Instrum. Methods Phys. Res. A **610**, 423–426 (2009).

[11]Y. Musienko, "Advances in multipixel Geiger-mode avalanche photodiodes (silicon photomultiplies)," Nucl. Instrum. Methods Phys. Res. A **598**, 213–216 (2009).

[12]K. J. Hong, Y. Choi, J. Kang, W. Hu, J. H. Jung, B. J. Min, Y. H. Chung, and C. Jackson, "Performance evaluation of a PET detector consists of a LYSO array coupled to a 4×4 array of large-size GAPD for MR compatible imaging," J. Instrum. **6**, P05012 (2011).

[13]C. Piemonte, "A new silicon photomultiplier structure for blue light detection," Nucl. Instrum. Methods Phys. Res. A **568**, 224–232 (2006).

[14]G. Llosá, N. Belcari, M. G. Bisogni, G. Collazuol, S. Marcatili, S. Moehrs, F. Morsani, C. Piemonte, and A. Del Guerra, "Energy and timing resolution studies with silicon photomultipliers (SiPMs) and 4-pixel SiPM matrices for PET," IEEE Trans. Nucl. Sci. **56**, 543–548 (2009).

[15]D. R. Schaart, H. T. van Dam, S. Seifert, R. Vinke, P. Dendooven, H. Löhner, and F. J. Beekman, "A novel, SiPM-array-based, monolithic scintillator detector for PET," Phys. Med. Biol. **54**, 3501–3512 (2009).

[16]T. Kato, J. Kataoka, T. Nakamori, T. Miura, H. Matsuda K. Sato, Y. Ishikawa, K. Yamamura, N. Kawabata, H. Ikeda, G. Sato, and K. Kamada, "Development of a large-area monolithic 4×4 MPPC array for a future PET scanner employing pixelized Ce:LYSO and Pr:LuAG crystals," Nucl. Instrum. Methods Phys. Res.A **638**, 83–91 (2011).
[17]S. Yamamoto, M. Imaizumi, T. Watabe, H. Watabe, Y. Kanai, E. Shimosegawa, and J. Hatazawa, "Development of a Si-PM-based high-resolution PET system for small animals," Phys. Med. Biol. **55**, 5817–5831 (2010).
[18]S. I. Kwon, J. S. Lee, H. S. Yoon, M. Ito, G. B. Ko, J. Y. Choi, S. H. Lee, I. C. Song, J. M. Jeong, D. S. Lee, and S. J. Hong, "Development of small-animal PET prototype using silicon photomultiplier (SiPM): Initial results of phantom and animal imaging studies," J. Nucl. Med. **52**, 572–579 (2011).
[19]J. H. Jung, Y. Choi, K. J. Hong, W. Hu, J. Kang, B. J. Min, S. H. Shin, H. K. Lim, Y. S. Huh, and E. J. Kim, "Development of a position decoder circuit for PET consisting of GAPD arrays," Nucl. Instrum. Methods Phys. Res. A **621**, 310–315 (2010).
[20]W. Hu, Y. Choi, K. J. Hong, J. Kang, J. H. Jung, Y. S. Huh, H. K. Lim, S. S. Kim, and B. T. Kim, "A simple and improved digital timing method for positron emission tomography," Nucl. Instrum. Methods Phys. Res. A **622**, 219–224 (2010).
[21]Y. C. Tai, A. Chatziioannou, S Siegel, J Young, D Newport, R. N. Goble, R. E. Nutt, and S. R. Cherry, "Performance evaluation of the microPET P4: A PET system dedicated to animal imaging," Phys. Med. Biol. **46**, 1845–1862 (2001).
[22]D. W. Townsend, T. Sprinks, T. Jones, A. Geissbuhle, M. Defrise, M. C. Gilardi, and J. Heather, "Three dimensional reconstruction of PET data from a multi-ring camera," IEEE Trans. Nucl. Sci. **36**, 1056–1065 (1989).
[23]D. Brasse, P. E. Kinahan, C. Lartizien, C. Comtat, M. Casey, and C. Michel, "Correction methods for random coincidences in fully 3D whole-body PET: impact on data and image quality," J. Nucl. Med. **46**(5), 859–867 (2005).
[24]H. Baghaei, Y. Zhang, H. Li, Y. Wang, S. Kim, R. A. Ramirez, J. Liu, S. Liu, and W. H. Wong, "GATE Monte Carlo simulation of a high-sensitivity and high-resolution LSO-based small animal PET camera," IEEE Trans. Nucl. Sci. **54**, 1568–1573 (2007).
[25]R. A. Ramirez, S. Liu, J. Liu, Y. Zhang, S. Kim, H. Baghaei, H. Li, Y. Wang, and W-H Won, "High-resolution L(Y)SO detectors using PMT-quadrant-sharing for human and animal PET cameras," IEEE Trans. Nucl. Sci. **55**, 862–869 (2008).
[26]P. D. Olcott, H. Peng, and C. S. Levin, "Novel electro-optical coupling technique for magnetic resonance-compatible positron emission tomography detectors," Mol. Imaging **8**(2), 74–86 (2009).
[27]U. Heinrichs, A. Blume, N. Bußmann, R. Engels, G. Kemmerling, S. Weber, and K. Ziemons, "Statistical studies on the light output and energy resolution of small LSO single crystals with different surface treatments combined with various reflector materials," Nucl. Instrum. Methods Phys. Res. A **486**, 60–66 (2002).
[28]J. H. Jung, Y. Choi, Y. H. Chung, O Devroede, M. Krieguer, P Bruyndonckx, and S. Tavernier, "Optimization of LSO/LuYAP phoswich detector for small animal PET," Nucl. Instrum. Methods Phys. Res. A **571**, 669–675 (2007).
[29]J. S. Karp, S. Surti, M. E. Daube-Witherspoon, R. Freifelder, C. A. Cardi, L. E. Adam, K. Bilger, and G. Muehllehner, "Performance of a brain PET camera based on anger-logic gadolinium oxyorthosilicate detectors," J. Nucl. Med. **44**(8), 1340–1349 (2003).
[30]H. P. Schlemmer, B. J. Pichler, M. Schmand, Z. Burbar, C. Michel, R. Ladebeck, K. Jattke, D. Townsend, C. Nahmias, P. K. Jacob, W. D. Heiss, and C. D. Claussen, "Simultaneous MR/PET imaging of the human brain: Feasibility study," Radiology **248**, 1028–1035 (2008).
[31]J. Kang, Y. Choi, K. J. Hong, J. H. Jung, W. Hu, Y. S. Huh, H. K. Lim, and B-T Kim, "A feasibility study of photosensor charge signal transmission to preamplifier using long cable for development of hybrid PET-MRI," Med. Phys. **37**, 5655–5664 (2010).
[32]S. P. Mok, C. H. Wang, J. C. Chen, and R. S. Liu, "Performance evaluation of a high resolution small animal PET scanner," Biomed. Eng. Appl. Basis Commun. **15**, 143–149 (2003).
[33]X. Liu and R. Lafores, "Quantitative small animal PET imaging with non-conventional nuclides," Nucl. Med. Biol. **36**, 551–559 (2009).
[34]R. S. Miyaoka, T. K. Lewellen, H. Yu, and D. L. McDaniel, "Design of a depth of interaction (DOI) PET detector module," IEEE Trans. Nucl. Sci. **45**, 1069–1073 (1998).
[35]Y. Shao, K. Meadors, R. W. Silverman, R. Farrell, L. Cirignano, R. Grazioso, K. S. Shah, and S. R. Cherry, "Dual APD array readout of LSO crystals: Optimization of crystal surface treatment," IEEE Trans. Nucl. Sci. **49**, 649–654 (2002).